Relativistic Interactions in the Radical Pair Model of Magnetic Field Sense in CRY-1 Protein of *Arabidopsis thaliana*

Artur F. Izmaylov* and John C. Tully

Department of Chemistry, Yale University, New Haven, Connecticut 06520

Michael J. Frisch

Gaussian, Inc., Wallingford, Connecticut 06492

Received: January 13, 2009; Revised Manuscript Received: August 20, 2009

Experimentally, it has been shown that magnetic field sensitivity in living organisms is connected to the presence of blue-light photoreceptor cryptochromes. Cryptochromes transduce a light signal through a chain of chemical reactions involving the formation of intermediate biradicals. It was proposed that an external magnetic field affects the interconversion between singlet and triplet states of biradicals and thus interferes with the signal transduction chain. Theoretical modeling of this process requires an accurate evaluation of all interactions important for singlet−triplet interconversion: electron−electron, spin−orbit, spin−spin, hyperfine, and Zeeman. In the current study we investigate these interactions at the CIS level of theory applied to representative fragments of the CRY-1 protein in the plant *Arabidopsis thaliana*. We find, in contrast to previous simplified modeling (O. Efimova, O.; Hore, P. J. *Biophys. J.* **2008**, *94*, 1565), that the spin−spin interaction is significantly larger than the "exchange" interaction. Thus it is not canceled by the latter but rather dies off with the inter-radical separation. Also, we find that the spin−orbit interaction can play a significant role in singlet−triplet interconversion for short inter-radical distances, and the hyperfine interaction becomes the only coupling interaction for long inter-radical distances.

I. Introduction

It is quite fascinating that some living organisms can sense even small changes in the surrounding magnetic field: migratory birds can orient themselves based on the inclination of Earth's magnetic field,[1,2] fruitflies (*Drosophila melanogaster*) can be trained to use a magnetic field to find food,[3] and even the plant *Arabidopsis thaliana* varies its hypocotyl growth rates due to magnetic field changes.[4] In the two latter cases it is still unclear why nature supplied these species with a magnetic sensing ability. Experimental studies across different species reveal several common features and similar conditions necessary for magnetic field sensing: the blue part of the light spectrum (470 nm or 2.67 eV) must be available, only the magnetic field inclination and intensity but not the polarity matter, and cryptochrome protein knockout mutants lose magnetic sensing ability. These features provided solid evidence for assigning the key role in this phenomenon to the blue-light photoreceptor proteins cryptochromes.[2−5] As implied by their name, cryptochromes' functional role had been a mystery for some time and was unraveled only two decades ago.[6] Currently, it is known that besides magnetic field sensing they regulate growth and development in plants and serve as circadian clocks in plants and animals. Another interesting feature of these proteins is their structural similarity with photolyases, enzymes responsible for repairing DNA damage from ultraviolet light.[6] It has also been found that some steps in the cryptochrome photoactivation mechanism are analogous to those in the photolyase repair mechanism.[6,7]

Recently, the X-ray structure of the photolyase homology domain of the *Arabidopsis* cryptochrome CRY-1 has become available.[8] This protein is deemed to be responsible for magnetic sensitivity in *Arabidopsis thaliana*.[4] Also, as shown by Solov'yov et al.[9] the DNA sequences of the cryptochrome genes in the migratory bird *Europian robin* and the plant *Arabidopsis thaliana* are very similar. Thus studying the CRY-1 protein is an important step to understanding magnetic sensing in general, and it will be a primary focus of the current work.

The basis for understanding the mechanism of the magnetic field influence is a radical pair model which is quite common for various magnetic field regulated reactions.[10−12] In this model, the essential part of the mechanism is the formation of a biradical intermediate that leads to different product channels based upon its spin-symmetry. An external magnetic field in the presence of other magnetic interactions (e.g., hyperfine) can affect the singlet−triplet states ratio and thus alter the yield of a specific product.[10]

Although some important details of the CRY-1 photoactivation mechanism are still unclear, the main steps are as follows. First, the pterin-based chromophore 5,10-methenyltetrahydrofolate absorbs blue light and transmits energy to the second flavin-based chromophore flavin adenine dinucleotide (FAD). After the indirect excitation, FAD is protonated either from a neighboring aspartic acid (Asp_{396})[7] or from a trapped water molecule[13] (see Scheme 1, $FADH^+$ mechanism). The excited $FADH^+$ cation accepts an electron from a neighboring tryptophan (Trp_{400}) and forms the radical pair of the neutral $FADH^\bullet$ and $Trp_{400}^{\bullet+}$ cation. Similar to photolyases, the CRY-1 protein has a chain of three tryptophan fragments near the FAD chromophore: Trp_{400}, Trp_{377}, and Trp_{324}. Therefore, further steps involve electron hops from the next tryptophan fragment (Trp_{377}) to the $Trp_{400}^{\bullet+}$ cation forming $FADH^\bullet-Trp_{377}^{\bullet+}$ biradical, and from Trp_{324} to the $Trp_{377}^{\bullet+}$ cation forming the $FADH^\bullet-Trp_{324}^{\bullet+}$ biradical. The deprotonation of the $Trp_{324}^{\bullet+}$ cation constitutes the final step in a crucial for magnetic sensing part of the CRY-1

10.1021/jp900357f CCC: $40.75
Published on Web 10/06/2009

SCHEME 1:

$FADH^+$ mechanism:

$$FAD^* + H^+ \rightarrow FADH^{+*}$$

$$FADH^{+*} + Trp_{400} \rightarrow FADH^{\bullet} + Trp^{+\bullet}_{400}$$

$$Trp^{+\bullet}_{400} + Trp_{377} \rightarrow Trp_{400} + Trp^{+\bullet}_{377}$$

$$Trp^{+\bullet}_{377} + Trp_{324} \rightarrow Trp_{377} + Trp^{+\bullet}_{324}$$

$$Trp^{+\bullet}_{324} \rightarrow Trp(dep)_{324} + H^+$$

$FAD^{\bullet -}$ mechanism:

$$FAD^* + Trp_{400} \rightarrow FAD^{-\bullet} + Trp^{+\bullet}_{400}$$

$$Trp^{+\bullet}_{400} + Trp_{377} \rightarrow Trp_{400} + Trp^{+\bullet}_{377}$$

$$Trp^{+\bullet}_{377} + Trp_{324} \rightarrow Trp_{377} + Trp^{+\bullet}_{324}$$

$$Trp^{+\bullet}_{324} \rightarrow Trp(dep)_{324} + H^+$$

$$FAD^{-\bullet} + H^+ \rightarrow FADH^{\bullet}$$

photoactivation mechanism. In order to incorporate the magnetic field influence into the considered mechanism, it is assumed that the back recombination of each biradical is possible only from the singlet state. Hence, if the magnetic field can alter the singlet−triplet ratio it also can affect the rates of the back reactions and facilitate signal transduction by increasing the yield of the final deprotonated product. This description of the photoactivation mechanism closely follows the theoretical interpretation of experimental works by Solov'yov et al.[9] and Efimova et al.[14] However, experimental results in refs 7, 15, and 16 as well as arguments presented by Kao et al.[13] for cryptochrome mechanisms in insects can lead to a different mechanism where electron hops precede the protonation of the FAD fragment (see Scheme 1, $FAD^{\bullet -}$ mechanism). Both mechanisms are plausible, and we are not aware of experimental results that clearly favor one or the other. For instance, a recent study by Bouly et al.[16] demonstrated that $FADH^{\bullet}$ is the signaling state, but the study was not detailed enough to attribute the $FADH^{\bullet}$ origin to $FAD^{\bullet -}$ or $FADH^+$. From a speculative perspective in both cases the first process facilitates the second: electron hops are energetically easier with the $FADH^+$ form, and the anionic form $FAD^{\bullet -}$ has a greater proton affinity than the initial FAD fragment. Structural similarities between photolyases and cryptochromes allow us to assign approximate time scale of 10−100 ns for the CRY-1 primary events depicted in Scheme 1; this estimate has been obtained for the *Escherichia coli* photolyase by Byrdin et al.[17] Although electron hops are usually faster events than proton transports, in this time scale both events are probable. In order to postpone choosing between these two paths until we have more detailed knowledge, in the current work we model both pathways.

In the system with two unpaired electrons that have equal *g*-factors, a magnetic field does not couple singlet and triplet states but only lifts the degeneracy of the triplet components. In order for an external magnetic field to influence the singlet−triplet transition, the system must have interactions which can either create a significant difference in *g*-factors for unpaired electrons or otherwise introduce a singlet−triplet coupling. The former factor is negligible considering the magnitude of the magnetic fields involved (≤5 G).[4] Thus, the key role is played by electron spins interacting with magnetic fields generated internally in spin−orbit, spin−spin, and nuclear hyperfine interactions.[18] It is instructive to split all interactions between singlet and triplet states into two groups: (1) ones which contribute to the singlet−triplet splitting without mixing states of different spin multiplicity (e.g., spin−spin and "exchange"), and (2) ones which couple states of different spin multiplicity (e.g., spin−orbit and hyperfine). The interplay between these two groups can be illustrated by mapping the singlet−triplet interconversion to single particle dynamics on the one-dimensional potential sketched in Figure 1. This mapping associates the first group of interactions to the difference between H_{aa} and H_{bb} (energy levels for uncoupled wells), while the coupling elements $H_{ab} = H_{ba}^*$ are related to the second group of interactions. If a particle is initially placed in well a, the wave function of the system at time t can be represented as a linear combination of stationary states of each well with time-dependent amplitudes C_a and C_b. Using a straightforward derivation,[19] the individual probabilities to find a particle in each well are

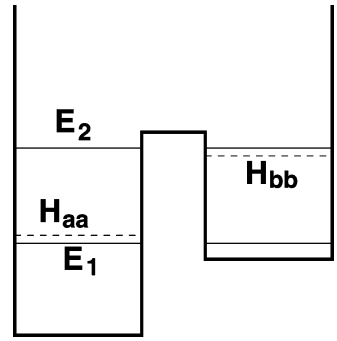

Figure 1. Double-well potential with a finite probability of tunneling. E_1 and E_2 (solid lines) are energies of the first two states, H_{aa} and H_{bb} (dashed lines) are ground state energies of individual wells as if there were no coupling.

$$|C_a|^2(t) = 1 - \frac{1 - \cos^2(\omega t)}{r^2 + 1} \quad (1)$$

$$|C_b|^2(t) = \frac{\sin^2(\omega t)}{r^2 + 1} \quad (2)$$

where

$$r = \frac{(H_{aa} - H_{bb})}{2H_{ab}} \quad (3)$$

$$\omega = \frac{2H_{ab}\sqrt{r^2 + 1}}{\hbar} \quad (4)$$

Here, the direct analogy of the singlet−triplet ratio is $|C_a|^2(t)/|C_b|^2(t)$. The magnetic field effect would be equivalent to adding a small energy contribution ϵ to the difference $H_{aa} - H_{bb}$ and corresponding change in the r parameter

$$r = \frac{(H_{aa} - H_{bb} + \epsilon)}{2H_{ab}} \quad (5)$$

Considering the infinitesimal field limit ($\epsilon \rightarrow 0$) the amplitude of both probabilities (eqs 1 and 2) is

$$\frac{1}{r^2 + 1} \rightarrow \frac{{H_{ab}}^2}{(H_{aa} - H_{bb})^2}\left[1 - \frac{2\epsilon}{H_{aa} - H_{bb}}\right] \quad (6)$$

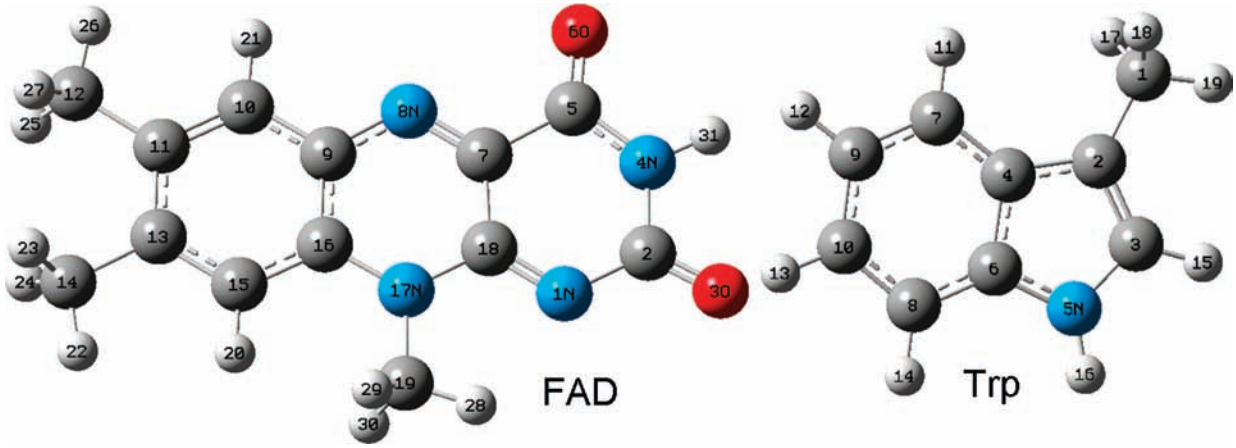

Figure 2. Model systems of the flavin adenine dinucleotide (FAD) and tryptophan (Trp) molecules. The FADH model is obtained by adding the hydrogen atom to atom 8N.

Thus, the effect of the Zeeman interaction (ϵ) becomes smaller for larger zero field splittings $H_{aa} - H_{bb}$, and thus the spin−spin and "exchange" interactions should not be more than an order of magnitude larger than the Zeeman interaction if we are to observe a non-negligible magnetic field effect. The spin−orbit and hyperfine interactions associated with the coupling element H_{ab} have a direct impact on the amplitude as well, but their contributions can also be damped by the splitting $H_{aa} - H_{bb}$ or, in other words, by the spin−spin and "exchange" interactions. This simple model vividly illustrates the importance of an accurate evaluation of both types of interactions to obtain an adequate description of the singlet−triplet interconversion dynamics. In previous work, some of these interactions were considered[9,14] but in a simplified manner and not systematically. Also, the spin−orbit interaction that potentially plays a crucial role in the singlet−triplet interconversion was neglected. Therefore, this work extends upon previous theoretical studies with a careful analysis of the main relativistic interactions at the same level of theory which provides grounds for subsequent dynamics simulations.

II. Theory

A. Models. We model active ingredients of the radical pair mechanism by the fragments depicted in Figure 2. The model of the tryptophan (Trp) fragment has been successfully used in previous studies by Himo et al.[20] and Lendzian et al.[21] to model hyperfine coupling constants of Trp residues in various biological systems. Trimming the FAD molecule is motivated by its orientation in the crystal structure[8] where the flavin ring system is the closest to the tryptophan chain part, and it is natural to expect that it plays the key role in the electron-hopping mechanism. Although our fragments are different from the real FAD and Trp molecules, we will refer to them as FAD and Trp for simplicity. For both mechanisms we consider two- and four-fragment models. The two-fragment model consists of three $FAD(H^+)-Trp_i$ pairs, where $i = 400$, 377, and 324. In the four-fragment model, the entire $FAD(H^+)-Trp_{400}-Trp_{377}-Trp_{324}$ chain is considered. All model fragments are optimized at the B3LYP/6-31G* level of theory and placed in the crystal structure orientation with respect to each other.[8] Clearly, the four-fragment model is more computationally demanding, and therefore it has been studied with the moderate 6-31G* basis set. The two-fragment model has also been explored with the larger EPR-II basis set[22] which is better suited for calculations of magnetic properties.[22,23] All calculations described in this paper are done with a development version of the Gaussian program.[24]

B. Method. As one of the computationally efficient methods that can describe spin-symmetry, low-lying excited states, and charge transfer (CT) excitations, at least on a qualitative level, the configuration interaction with single excitations (CIS) method has been chosen. Another nice feature of the CIS approach is its straightforward atomic orbital (AO) direct formulation which allows one to treat very large systems.[25] The "exchange" interaction can be directly extracted from CIS calculations as an energy difference between singlet and triplet CT states. In order to distinguish the CT solutions from other excited states, we employed the Mulliken charge analysis of excited state densities. There are three main relativistic interactions that depend explicitly on the electron spin variables: spin−spin (SS), spin−orbit (SO), and hyperfine (HF). For all interactions we start from corresponding terms of the Breit−Pauli (BP) Hamiltonian.[26,27] In order to estimate individual contributions, we use perturbation theory (PT) to obtain parameters of standard phenomenolgical Hamiltonians for each interaction treated as perturbation.

1. The Spin−Spin Interaction. The SS interaction appears in systems with $S \geq 1$, and it lifts the degeneracy corresponding to states with different M_S. In our case, it contributes to the splitting of CT triplet components. The SS BP Hamiltonian[26] can be written as a sum of the Fermi-contact term

$$\hat{H}_{SS}^{(FC)} = -\frac{4\pi\alpha^2}{3}\sum_{i\neq j}\delta(\mathbf{r}_{ij})\hat{\mathbf{s}}(i)\hat{\mathbf{s}}(j) \tag{7}$$

and the dipole−dipole term

$$\hat{H}_{SS}^{(DD)} = \frac{\alpha^2}{2}\sum_{i\neq j}\left[\frac{\hat{\mathbf{s}}(i)\hat{\mathbf{s}}(j)}{r_{ij}^3} - \frac{3(\hat{\mathbf{s}}(i)\mathbf{r}_{ij})(\hat{\mathbf{s}}(j)\mathbf{r}_{ij})}{r_{ij}^5}\right] \tag{8}$$

Here, $\alpha \approx 1/137$ is the fine structure constant, indices i and j enumerate electrons, $\hat{\mathbf{s}}(i)$ is the one-electron spin operator, and $\mathbf{r}_{ij}$ is the interelectron coordinate. The quadratic form of the SS BP Hamiltonian with respect to the spin coordinates allows us to substitute these terms by the phenomenological or spin Hamiltonian within the triplet subspace

$$\hat{\mathscr{H}}_{SS} = \hat{\mathbf{S}}\mathbf{D}\hat{\mathbf{S}} \tag{9}$$

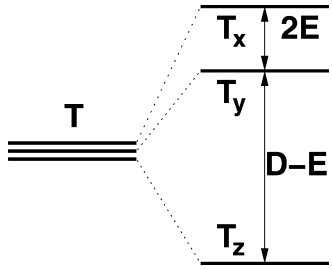

Figure 3. Relation between (D,E) parameters of eq 12 and the first-order spin−spin splitting of a triplet state.

where $\hat{\mathbf{S}}$ is the many-electron spin operator, and $\mathbf{D}$ is the traceless tensor

$$D_{lk} = \frac{\alpha^2}{2}\langle T^{+1}|\sum_{i\neq j}\frac{[\delta_{lk}r_{ij}^{\ 2} - 3(\mathbf{r}_{ij})_l(\mathbf{r}_{ij})_k]}{r_{ij}^{\ 5}}[2\hat{s}_z(i)\hat{s}_z(j) - \hat{s}_x(i)\hat{s}_x(j) - \hat{s}_y(i)\hat{s}_y(j)]|T^{+1}\rangle \quad (10)$$

calculated with the high-spin triplet wave function $|T^{+1}\rangle$. The spin Hamiltonian can be transformed to the principle axes (X,Y,Z) where

$$\hat{\mathscr{H}}_{SS} = D_{XX}S_X^{\ 2} + D_{YY}S_Y^{\ 2} + D_{ZZ}S_Z^{\ 2} \quad (11)$$

or to the more common spherical-tensor form[27−30]

$$\hat{\mathscr{H}}_{SS} = D\left[\hat{S}_0^{\ 2} - \frac{1}{3}\hat{S}^2\right] + E[\hat{S}_+^{\ 2} + \hat{S}_-^{\ 2}] \quad (12)$$

with spherical-tensor operators defined as

$$\hat{S}_+ = -\frac{\hat{S}_X + i\hat{S}_Y}{\sqrt{2}} \quad (13)$$

$$\hat{S}_0 = \hat{S}_Z$$

$$\hat{S}_- = \frac{\hat{S}_X - i\hat{S}_Y}{\sqrt{2}}$$

Parameters D and E in eq 12 can be expressed as

$$D = \frac{3D_{ZZ}}{2} \quad (14)$$

$$E = \frac{1}{2}(D_{XX} - D_{YY}) \quad (15)$$

and their relation to the SS splitting of the triplet levels is illustrated by Figure 3. Essentially, the diagonalization of the spin Hamiltonian $\mathscr{H}$ or $\mathbf{D}$ tensor is equivalent to that of the BP Hamiltonian in the triplet subspace, and therefore, parameters D and E are used to assess the first-order PT contribution of the SS interaction.

In general, calculating matrix elements with the SS BP operators (eq 10) would require either forming two-particle density matrices or using the resolution of the identity technique.[28] Although the CIS two-particle density matrix can be written in terms of one-particle densities,[31] here we use an even simpler approach of the mean-field approximation (MFA) where the CIS wave function is treated as if it were a single determinant, and hence only a one-particle density matrix of an excited state is sufficient for the $\mathbf{D}$ tensor evaluation. The error introduced by this approximation is considered small.[29,30,32] The $\mathbf{D}$ tensor within the MFA can be obtained by contracting the one-particle spin density of the CT triplet state ($\mathbf{P}^{(\alpha-\beta)}$) with the appropriate two-electron integrals

$$D_{kl} = \frac{\alpha^2}{2}\sum_{\mu\nu\lambda\sigma}[P_{\mu\nu}^{\ (\alpha-\beta)}P_{\lambda\sigma}^{\ (\alpha-\beta)} - P_{\mu\sigma}^{\ (\alpha-\beta)}P_{\lambda\nu}^{\ (\alpha-\beta)}]\langle\mu\nu|r_{12}^{\ -5}\{\delta_{kl}r_{12}^{\ 2} - 3(\mathbf{r}_{12})_k(\mathbf{r}_{12})_l\}|\lambda\sigma\rangle \quad (16)$$

where μ, ν, λ, and σ are Gaussian AOs. Another simplification originating from MFA is a cancellation of the SS Fermi-contact component

$$D_{kl}^{(FC)} = \frac{4\pi\alpha^2\delta_{kl}}{3}\sum_{\mu\nu\lambda\sigma}[P_{\mu\nu}^{\ (\alpha-\beta)}P_{\lambda\sigma}^{\ (\alpha-\beta)} - P_{\mu\sigma}^{\ (\alpha-\beta)}P_{\lambda\nu}^{\ (\alpha-\beta)}]\langle\mu\nu|\delta(\mathbf{r}_{12})|\lambda\sigma\rangle \quad (17)$$

because of the permutational symmetry of the overlap integrals ($\langle\mu\nu|\delta(\mathbf{r}_{12})|\lambda\sigma\rangle = \langle\mu\sigma|\delta(\mathbf{r}_{12})|\lambda\nu\rangle$). Using this permutational symmetry eq 16 can be rewritten as[27]

$$D_{kl} = \frac{\alpha^2}{2}\sum_{\mu\nu\lambda\sigma}[P_{\mu\nu}^{\ (\alpha-\beta)}P_{\lambda\sigma}^{\ (\alpha-\beta)} - P_{\mu\sigma}^{\ (\alpha-\beta)}P_{\lambda\nu}^{\ (\alpha-\beta)}] \times \left(\frac{\partial}{\partial R_k^{(\mu)}} + \frac{\partial}{\partial R_k^{(\nu)}}\right)\left(\frac{\partial}{\partial R_l^{(\lambda)}} + \frac{\partial}{\partial R_l^{(\sigma)}}\right)\langle\mu\nu|r_{12}^{\ -1}|\lambda\sigma\rangle \quad (18)$$

where $\mathbf{R}^{(\mu)}$,$\mathbf{R}^{(\nu)}$,$\mathbf{R}^{(\lambda)}$ and $\mathbf{R}^{(\sigma)}$ are centers of Gaussian AOs μ, ν, λ, and σ, respectively. Thus, calculation of $\mathbf{D}$ elements requires contractions similar to those required in direct Hartree−Fock second derivative calculations.

2. The Spin−Orbit Interaction. The SO part of the BP Hamiltonian also contains one- and two-electron terms[26]

$$\hat{H}_{BP} = \hat{H}_{BP1} + \hat{H}_{BP2} \quad (19)$$

$$\hat{H}_{BP1} = \frac{\alpha^2}{2}\sum_{i,N}\frac{Z_N}{r_{iN}^{\ 3}}[\hat{\mathbf{r}}_{iN}\times\hat{\mathbf{p}}(i)]\hat{\mathbf{s}}(i) \quad (20)$$

$$\hat{H}_{BP2} = -\frac{\alpha^2}{2}\sum_i\sum_{i\neq j}\frac{1}{r_{ij}^{\ 3}}[\hat{\mathbf{r}}_{ij}\times\hat{\mathbf{p}}(i)]\hat{\mathbf{s}}(i) + \frac{2}{r_{ij}^{\ 3}}[\hat{\mathbf{r}}_{ij}\times\hat{\mathbf{p}}(j)]\hat{\mathbf{s}}(i) \quad (21)$$

where index N enumerates nuclei, Z_N is the nuclear charge, $\hat{\mathbf{p}}(i)$ is the one-electron momentum operator, and $\mathbf{r}_{iN}$ is the electron−nuclear coordinate. In order to eliminate the computational cost related to the two-electron component of the SO BP Hamiltonian, we use an effective one-electron spin−orbit operator

$$\hat{H}_{SO} = \frac{\alpha^2}{2} \sum_{i,N} \frac{Z_N^{eff}}{r_{iN}^3} [\hat{\mathbf{r}}_{iN} \times \hat{\mathbf{p}}(i)] \hat{\mathbf{s}}(i) \quad (22)$$

where Z_N^{eff} is an effective charge of nucleus N and the difference $Z_N^{eff} - Z_N$ accounts for the missing two-electron SO contribution in eq 22.[33]

In terms of PT, generally, the SO interaction contributes to the second order, but in the case of small nonrelativistic singlet−triplet splittings it can contribute to the first order as well. In our case of spatially separated radical pairs, the singlet−triplet CIS gaps are quite tiny (see below); therefore, the SO contribution is considered within the second and first orders of quasi-degenerate PT.[29,34] The Hermitian SO perturbation matrix up to the second order is

$$\langle \Phi_I | \hat{H}_{SO}^{(1-2)} | \Phi_J \rangle = \langle \Phi_I | \hat{H}_{SO} | \Phi_J \rangle + \frac{1}{2} \sum_P \langle \Phi_I | \hat{H}_{SO} | \Phi_P \rangle \langle \Phi_P | \hat{H}_{SO} | \Phi_J \rangle \left[\frac{1}{E_I - E_P} + \frac{1}{E_J - E_P} \right] \quad (23)$$

where Φ_I and Φ_J are CT states of interest (singlet and three components of triplets), Φ_P's are other CIS solutions, and E_I, E_J, and E_P are the corresponding CIS energies. The second-order sum over states in eq 23 has been substituted in actual calculations by a sum over the first 60 excited states. Only the triplet states with $M_S = 0$ are formed in our CIS calculations; thus, to evaluate all matrix elements of the $\hat{H}_{SO}$ operator in eq 23 we use the Wigner−Eckart theorem[34] for the singlet−triplet couplings and in addition spin shift operators ($\hat{\mathbf{S}}_{\pm}$) for the triplet−triplet couplings. In order to present our study in a more concise manner, 16 matrix elements of the SO perturbation matrix (eq 23) are gathered into three groups: (1) the singlet−singlet element that shifts the singlet energy, (2) the singlet−triplet block that creates the coupling, and (3) the triplet−triplet block which acts similarly as the first-order SS contribution. Because of this similarity, the SO and SS corrections to the splitting of the triplet components are considered together by adding the SO triplet−triplet block to the **D** tensor prior to its diagonalization. It is worth mentioning that because of the difference in spin-symmetry of involved states, the SO triplet−triplet block cannot be directly summed with the **D** tensor and needs to be transformed first. Appropriate transformations have been described for the general case of arbitrary spin states by Neese et al.[35] However, in our case of $S = 1$, we take a simpler approach: the SO triplet−triplet block requires only a unitary transformation from the spherical-tensor basis to the Cartesian basis to be summed directly with the **D** tensor.

3. The Hyperfine Interaction. The HF term originates from interactions of electron spins with spins of magnetic nuclei. The corresponding Hamiltonian can be split into the isotropic (or spherically symmetric)

$$\hat{H}_{HF}^{(iso)} = g_e \beta_e \frac{8\pi}{3} \sum_{i,N} g_N \beta_N \hat{\mathbf{s}}(i) \hat{\mathbf{I}}(N) \delta(\mathbf{r}_{iN}) \quad (24)$$

and the dipolar (or anisotropic)

$$\hat{H}_{HF}^{(dip)} = -g_e \beta_e \sum_{i,N} g_N \beta_N \left[\frac{\hat{\mathbf{s}}(i)\hat{\mathbf{I}}(N)}{r_{iN}^3} - \frac{3(\hat{\mathbf{s}}(i)\mathbf{r}_{iN})(\hat{\mathbf{I}}(N)\mathbf{r}_{iN})}{r_{iN}^5} \right] \quad (25)$$

TABLE 1: Characteristics of CT States for the FAD$^{\bullet-}$ Mechanism Calculated with the CIS Method

states		Mulliken charges, a.u.			
spin	energy, eV	FAD	Trp_{400}	Trp_{377}	Trp_{324}
		Two-Fragment Model/6-31G*			
T	6.1307	−1.002	1.002		
S	6.1313	−1.000	1.000		
T	6.7697	−1.006		1.006	
S	6.7697	−0.994		0.994	
T	7.0880	−0.968			0.968
S	7.0880	−1.032			1.032
		Two-Fragment Model/EPR-II			
T	6.1017	−0.921	0.921		
S	6.0816	−0.843	0.843		
T	6.7419	−1.000		1.000	
S	6.7419	−1.000		1.000	
T	6.9173	−1.001			1.001
S	6.9173	−0.999			0.999
		Four-Fragment Model/6-31G*			
T	6.0889	−1.004	0.994	0.009	0.001
S	6.0905	−0.870	0.861	0.008	0.001
T	6.6997	−1.005	0.058	0.946	0.001
S	6.6997	−1.005	0.057	0.947	0.001
T	7.1688	−1.004	0.003	0.001	1.000
S	7.1688	−1.006	0.003	0.001	1.002

parts. Here, $\hat{\mathbf{I}}(N)$ is the nuclear spin operator, g_e, g_N, β_e, and β_N are g-factors and Bohr magnetons for electrons and nuclei. Using the same approach as in the SS case, the HF spin Hamiltonian can be written as

$$\hat{\mathscr{H}}_{HF} = \hat{\mathbf{S}} \mathbf{A} \hat{\mathbf{I}} \quad (26)$$

where $\hat{\mathbf{I}}$ is many nuclear spin operator and **A** is the HF coupling tensor. **A** components for each nuclei can be further split into two parts: the isotropic

$$A_{N,kl}^{(iso)} = \delta_{kl} \frac{8\pi}{3} \frac{g_e g_N \beta_e \beta_N}{\langle \Phi | S_z | \Phi \rangle} \langle \Phi | \sum_i \delta(\mathbf{r}_{iN}) \hat{s}_z(i) | \Phi \rangle \quad (27)$$

and the dipolar

$$A_{N,kl}^{(dip)} = \frac{g_e g_N \beta_e \beta_N}{\langle \Phi | S_z | \Phi \rangle} \langle \Phi | \sum_i \left[\frac{\delta_{kl}}{r_{iN}^3} - \frac{3(\mathbf{r}_{iN})_k (\mathbf{r}_{iN})_l}{r_{iN}^5} \right] \hat{s}_z(i) | \Phi \rangle \quad (28)$$

where kl are Cartesian components and $|\Phi\rangle$ is an electron wave function with nonzero S_z. As in the SS case, contractions (27) and (28) are done with the CT triplet state $\mathbf{P}^{(\alpha-\beta)}$ densities and corresponding one-electron integrals. Usually, the HF interaction is considered within the first order of PT,[27] and thus in the current study components of the HF coupling tensor **A** will be used to assess the HF contribution.

III. Results and Discussions

Tables 1 and 2 present energies and Mulliken charges on each fragment of the lowest CT states for both mechanisms. The CT states have such a pronounced difference in charge distribution compared to other states that we would not expect a change in the assignment of CT states due to using any other standard scheme for extracting partial charges. Two- and four-fragment

TABLE 2: Characteristics of CT states for the $FADH^+$ mechanism calculated with the CIS method

states		Mulliken charges, a.u.			
spin	energy, eV	FADH	Trp_{400}	Trp_{377}	Trp_{324}
Two-Fragment Model/6-31G*					
T	2.8125	−0.003	1.003		
S	2.8123	−0.008	1.008		
T	2.6033	0.003		0.997	
S	2.6033	−0.003		1.003	
T	2.5570	0.001			0.999
S	2.5570	−0.001			1.001
Two-Fragment Model/EPR-II					
T	2.9027	−0.001	1.001		
S	2.9029	−0.011	1.011		
T	2.6806	0.000		1.000	
S	2.6806	0.000		1.000	
T	2.6349	0.000			1.000
S	2.6349	0.000			1.000
Four-Fragment Model/6-31G*					
T	2.6131	−0.008	0.001	0.915	0.092
S	2.6132	−0.009	0.001	0.916	0.091
T	2.7367	−0.009	0.003	0.005	1.001
S	2.7367	−0.009	0.003	0.005	1.001
T	2.7619	−0.008	0.914	0.093	0.001
S	2.7624	0.004	0.903	0.092	0.001

models produce qualitatively similar results. On the other hand, the two studied mechanisms have significantly different excitation energies. Energies required for the electron hopping in the $FADH^+$ mechanism (Table 2) correspond exactly to the blue part of the visible light spectrum (470 nm or 2.67 eV), while those in the $FAD^{\bullet-}$ mechanism are beyond the visible range (<3.30 eV). Also, in the case of $FADH^+$, long-distance radical pairs have lower energies (except in the case of the four-fragment model where the middle $Trp_{377}^{\bullet+}$ configuration has the lowest energy). Thus initial excitation of the closest CT radical-pair propagates further without an additional energy cost. This trend is completely reversed in the $FAD^{\bullet-}$ case. The basis set extension leads only to minor changes in excitation energies and less pronounced charge transfer for the short-distance $FAD^{\bullet-}-Trp_{400}^{\bullet+}$ pair. We attribute the latter feature to a larger overlap of the fragments' electron densities when the EPR-II basis is employed. Although we have not included the protein environment in our study, the energy difference between the two mechanisms strongly suggests that the initial protonation is a necessary condition for the electron hopping. However, we would like to postpone an ultimate answer to the question about the mechanism until a more thorough study which includes the protein environment is performed. Hence, here we investigate the interactions which might be important in either mechanism.

Tables 3 and 4 present characteristics of the main interactions affecting the interconversion between the lowest CT singlet and triplet states. The "exchange" interaction or simply the CIS singlet−triplet gap is quite small in most of the cases. It has a very fast spatial decay and, therefore, can be safely neglected for the second (Trp_{377}) and third (Trp_{324}) radical pairs.

The main contribution to the triplet−triplet splitting comes from the first-order SS interaction which has significant values for the first two pairs (Trp_{400} and Trp_{377}) in the four-fragment models and for all three pairs in the two-fragment models. The spatial decay of the D parameter (eq 12) has a $1/R^{3.24}$ form for $FADH^{\bullet}-Trp^{\bullet+}$ and a $1/R^{3.34}$ form for $FAD^{\bullet-}-Trp^{\bullet+}$ in the two-fragment/6-31G* model, where R is the distance between the fragments' center of masses.[36] This behavior is very similar to the classical $1/R^3$ decay for the magnetic dipole−dipole interaction. In contrast, the D parameter in the four-fragment model has much faster spatial decay that does not follow the simple classical relation. We attribute this to electron screening which attenuates the SS interaction in the four-fragment model. Another contribution to the triplet−triplet splitting comes from the second-order SO terms (eq 23). For the Trp_{400} and Trp_{377} biradicals, the SO corrected values of D and E parameters (eq 12) are of the same order of magnitude as the initial first order SS values. Owing to the second-order structure, the SO interaction contributes even for the most distant fragments because of couplings with local triplets which are energetically close to the triplet states of interest. The same effect can be seen for the singlet−singlet SO term (eq 23) that reduces the singlet state energy. The calculated SO singlet−triplet couplings have significant values only for the closest Trp_{400} biradical, and generally, the SO interaction is much weaker for the $FADH^+$ mechanism than for the $FAD^{\bullet-}$ counterpart. The hyperfine coupling constants are even smaller than the $FADH-Trp_{400}^{\bullet+}$ pair SO couplings, but because of a locality of the hyperfine interaction, the hyperfine couplings do not decay with the inter-radical distance. Also, they undergo only minor changes between different models and mechanisms.

Comparison of the CIS hyperfine isotropic constants for the Trp part with those obtained in experiment[37] ($A^{(iso)} = 14.2$ G for H17(Trp)) indicates that the CIS method underestimates hyperfine constants almost by a factor of 2. The experimental results are in a better agreement with the unrestricted B3LYP/EPR-II method ($A^{(iso)} = 17.5$ G for H17(Trp)), while the restricted open-shell version of B3LYP produces results similar to those obtained with CIS. On the other hand, Sinnecker and Neese have demonstrated[32] that the unrestricted B3LYP (UB3LYP) method usually overestimates the electron spin−spin tensor components, and the restricted open-shell version corrects for this overestimation. Also, quantities like spin−orbit and "exchange" couplings are not well-defined within the unrestricted single-determinant framework. Taking into account these limitations of the UB3LYP and CIS methods, we consider the CIS results as qualitatively accurate for all properties but hyperfine couplings where the UB3LYP/EPR-II estimates are more realistic. Owing to local character of the hyperfine interaction, the UB3LYP estimations for hyperfine couplings in the excited CT states are done by considering the individual $FADH^{\bullet}(FAD^{\bullet-})$ and $Trp^{\bullet+}$ radicals in their ground states (see captions to Tables 3 and 4).

Overall, the basis extension in the two-fragment model does not significantly affect results for the second and third tryptophan pairs. Therefore, we assume that the four-fragment/6-31G* model provides reliable estimates for the second and third tryptophan pairs which would undergo only minor changes if a larger basis set were used. According to the four-fragment/6-31G* model, in both mechanisms the only significant interaction in the third radical pair is the hyperfine interaction, and the second radical pair has the triplet−triplet splitting comparable to the hyperfine contribution. Hence, in both radical pairs, the singlet−triplet interconversion takes place and even weak magnetic fields 1−5 G[38] can affect it. Results from different models are less similar in the case of the nearest radical pair, but due to larger SO singlet−triplet couplings, the $FAD^{\bullet-}$ mechanism has a greater potential for the singlet−triplet interconversion than the $FADH^+$ mechanism. Although in the latter case the singlet−triplet interconversion cannot be totally discarded, the effect of a weak magnetic field will be probably negligible (see eq 6) because of much greater spin−triplet energy splittings.

TABLE 3: Interactions between FADH$^{\bullet}$ and Trp$^{\bullet+}$ Radicals Calculated with the CIS Method[a]

interaction	Trp_{400}	Trp_{377}	Trp_{324}
	Two-Fragment Model/6-31G*		
"exchange", $E_S - E_T$	−1.7	0.0	0.0
$SS^{(1)}(SS^{(1)} + SO^{(2)})$, D	105.7(109.2)	21.4(24.3)	7.2(9.4)
$SS^{(1)}(SS^{(1)} + SO^{(2)})$, E	4.7(4.7)	0.3(0.2)	0.0(0.3)
$SO^{(2)}$, S−S coupling	−0.7	−0.7	−0.7
$SO^{(1-2)}$, S−T coupling	5.6	0.0	0.0
$A_{max}^{(iso)}$	7.4	7.2	7.2
$A_{max}^{(dip)}$	−3.2/−3.0/6.3	−3.3/−3.0/6.3	−3.3/−3.0/6.3
	Two-Fragment Model/EPR-II		
"exchange", $E_S - E_T$	1.9	0.0	0.0
$SS^{(1)}(SS^{(1)} + SO^{(2)})$, D	111.0(116.4)	21.4(25.7)	7.2(10.5)
$SS^{(1)}(SS^{(1)} + SO^{(2)})$, E	5.2(5.0)	0.3(0.5)	0.0(0.3)
$SO^{(2)}$, S−S coupling	−1.2	−1.0	−1.0
$SO^{(1-2)}$, S−T coupling	14.2	0.0	0.0
$A_{max}^{(iso)}$	8.0	7.8	7.8
$A_{max}^{(dip)}$	−3.4/−3.1/6.5	−3.4/−3.2/6.6	−3.4/−3.2/6.6
	Four-Fragment Model/6-31G*		
"exchange", $E_S - E_T$	−4.4	0.6	0.0
$SS^{(1)}(SS^{(1)} + SO^{(2)})$, D	83.2(85.8)	8.3(10.0)	0.0(2.3)
$SS^{(1)}(SS^{(1)} + SO^{(2)})$, E	8.1(8.2)	0.4(0.5)	0.0(0.0)
$SO^{(2)}$, S−S coupling	−0.6	−0.5	−0.7
$SO^{(1-2)}$, S−T coupling	14.0	1.4	0.0
$A_{max}^{(iso)}$	6.6	7.0	7.2
$A_{max}^{(dip)}$	−3.3/−3.0/6.3	−3.3/−3.1/6.3	−3.3/−3.1/6.3

[a] All values are in 10^{-4} cm^{-1} (1 G ≈ 0.93 × 10^{-4} cm^{-1}). Distances between center of masses in FADH$^{\bullet}$−Trp$^{\bullet+}$ pairs are 8.4, 13.2, and 19.3 Å for Trp_{400}, Trp_{377}, and Trp_{324}, respectively. The SO singlet−triplet coupling is given by the Euclidian norm of the $(\langle S|\hat{H}_{SO}^{(1-2)}|T^{+1}\rangle, \langle S|\hat{H}_{SO}^{(1-2)}|T^{0}\rangle, \langle S|\hat{H}_{SO}^{(1-2)}|T^{-1}\rangle)$ vector. The largest hyperfine coupling constant corresponds to H17(Trp) and N8(FADH) for isotropic and dipolar components, respectively.[41] The corresponding UB3LYP/EPR-II values are H17(Trp) $A^{(iso)}$ = 17.5 G and N8(FAD) $A^{(dip)}$ = −4.6/−4.4/9.0 G.

TABLE 4: Interactions between FAD$^{\bullet-}$ and Trp$^{\bullet+}$ Radicals Calculated with the CIS Method[a]

interaction	Trp_{400}	Trp_{377}	Trp_{324}
	Two-Fragment Model/6-31G*		
"exchange", $E_S - E_T$	−5.0	0.0	0.0
$SS^{(1)}(SS^{(1)} + SO^{(2)})$, D	118.4(128.6)	22.7(24.9)	8.0(10.0)
$SS^{(1)}(SS^{(1)} + SO^{(2)})$, E	4.7(3.8)	0.3(0.3)	0.0(0.0)
$SO^{(2)}$, S−S coupling	−8.0	−0.6	−0.6
$SO^{(1-2)}$, S−T coupling	31.2	0.0	0.0
$A_{max}^{(iso)}$	8.0	7.2	7.0
$A_{max}^{(dip)}$	−3.1/−3.0/6.1	−3.2/−3.1/6.3	−3.3/−3.2/6.5
	Two-Fragment Model/EPR-II		
"exchange", $E_S - E_T$	−162.1	0.0	0.0
$SS^{(1)}(SS^{(1)} + SO^{(2)})$, D	110.1(119.2)	22.5(22.8)	7.7(9.2)
$SS^{(1)}(SS^{(1)}+SO^{(2)})$, E	4.1(3.8)	0.3(0.5)	0.0(0.2)
$SO^{(2)}$, S−S coupling	−13.6	0.0	0.0
$SO^{(1-2)}$, S−T coupling	436.3	0.0	0.0
$A_{max}^{(iso)}$	8.6	7.8	7.8
$A_{max}^{(dip)}$	−2.8/−2.7/5.6	−3.3/−3.2/6.5	−3.4/−3.2/6.6
	Four-Fragment Model/6-31G*		
"exchange", $E_S - E_T$	−12.7	−0.2	0.0
$SS^{(1)}(SS^{(1)} + SO^{(2)})$, D	98.1(100.3)	5.1(6.8)	0.0(2.1)
$SS^{(1)}(SS^{(1)}+SO^{(2)})$, E	3.0(2.4)	0.1(0.1)	0.0(0.0)
$SO^{(2)}$, S−S coupling	−126.4	−0.5	0.0
$SO^{(1-2)}$, S−T coupling	121.5	2.0	0.0
$A_{max}^{(iso)}$	8.2	7.0	7.0
$A_{max}^{(dip)}$	−3.1/−3.0/6.1	−3.2/−3.1/6.3	−3.2/−3.1/6.3

[a] All values are in 10^{-4} cm^{-1} (1 G ≈ 0.93 × 10^{-4} cm^{-1}). Distances between center of masses in FAD$^{\bullet-}$−Trp$^{\bullet+}$ pairs are 8.4, 13.2, and 19.3 Å for Trp_{400}, Trp_{377}, and Trp_{324}, respectively. The SO singlet−triplet coupling is given by the Euclidian norm of the $(\langle S|\hat{H}_{SO}^{(1-2)}|T^{+1}\rangle, \langle S|\hat{H}_{SO}^{(1-2)}|T^{0}\rangle, \langle S|\hat{H}_{SO}^{(1-2)}|T^{-1}\rangle)$ vector. The largest hyperfine coupling constant corresponds to H17(Trp) and N8(FAD) for isotropic and dipolar components, respectively.[41] The corresponding UB3LYP/EPR-II values are H17(Trp) $A^{(iso)}$ = 17.5 G and N8(FAD) $A^{(dip)}$ = −5.0/−5.0/10.0 G.

Previously, based on a simple scaling analysis and semiempirical modeling, Efimova et al. concluded that the "exchange" and SS interactions are quite significant for the FADH$^{\bullet}$−Trp$^{\bullet+}$ pairs; however they do not suppress the singlet−triplet interconversion because of their mutual cancellation. According to our results, this fortuitous cancellation does not take place but rather the spin−spin interaction is larger than the "exchange" interaction at all distances, and both interactions decay fast

enough to become negligible for the most distant $FADH^{\bullet}-Trp_{324}^{\bullet+}$ pair (see Table 3, four-fragment model). Recently, Biskup et al. have estimated values of "exchange" and spin−spin coupling for the $FADH^{\bullet}-Trp_{324}^{\bullet+}$ biradical in the X/Cry-DASH protein from its transient EPR spectrum.[39] Their estimates $D = -3.6$ G and $J = 2.4$ G are in a better agreement with those of Efimova et al. rather than with our values. We see two possible reasons for this: First, the "exchange" interaction could have a slower exponential decay with the inter-radical distance in the protein environment than in vacuum; thus our approach can underestimate the J value by neglecting environmental effects. In contrast, use of some empirical constants for a generic protein environment allows Efimova et al. to account for environmental effects up to a certain extent. Second, D and J parameters cannot be measured directly in experiment, and an extraction procedure can have its own level of uncertainty due to the presence of other interactions (e.g., inhomogeneous broadening because of the hyperfine interaction[40]).

IV. Conclusions

Our study demonstrates that among two possible mechanisms of the CRY-1 photoactivation, the mechanism with initial protonation of the FAD chromophore requires an amount of energy for the subsequent electron hopping that corresponds exactly to the blue part of the light spectrum. Thus, our results suggest that the $FADH^{+}$ mechanism is preferred over the mechanism with the initial electron hopping and the subsequent $FAD^{\bullet-}$ protonation.

Relativistic and "exchange" interactions estimated in this work confirmed that a weak magnetic field can affect the singlet−triplet ratio for the most distant biradicals in both mechanisms, because only the local hyperfine interaction is non-negligible at such separation. However, this is not a result of mutual cancellation of the spin−spin and "exchange" contributions but rather is a consequence of their individual spatial decay.

The magnitude of the hyperfine coupling constants ($A_{max}^{(iso)} = 17.5$ G) suggests that artificial magnetic fields (1−5 G) involved in experiments with *Arabidopsis thaliana* can affect the signal transduction rate. On the other hand, hyperfine interactions in the $FADH^{\bullet}-Trp^{\bullet+}$ biradicals are much stronger than the Zeeman interaction with the magnetic field of the Earth (≈0.5 G). Therefore, an alternative mechanism for the bird avian compass has been proposed very recently.[42−44] This mechanism involves radicals with weaker hyperfine interactions ($O_2^{\bullet-}$ and $FADH^{\bullet}$), and thus, it could be more plausible for explaining incredible sensitivity of some living species to even tiny changes in the magnetic field.

Consideration of the spin−orbit interaction using quasi-degenerate perturbation theory up to the second order revealed its significance to the coupling elements between singlet and triplet states and, thus, its importance for future simulations of dynamics in the CRY-1 protein.

Acknowledgment. A.F.I. appreciates helpful discussions with H. P. Hrant, N. Shenvi, A. V. Zaitsevskii, and R. P. Steele. This work was financially supported by Gaussian, Inc.

References and Notes

(1) Ritz, T.; Thalau, P.; Phillips, J. B.; Wiltschko, R.; Wiltschko, W. *Nature* **2004**, *429*, 177.

(2) Mouritsen, H.; Janssen-Bienhold, U.; Liedvogel, M.; Feenders, G.; Stalleicken, J.; Dirks, P.; Weiler, R. *Proc. Natl. Acad. Sci. U.S.A.* **2004**, *101*, 14294.

(3) Gegear, R. J.; Casselman, A.; Waddell, S.; Reppert, S. M. *Nature* **2008**, *454*, 1014.

(4) Ahmad, M.; Galland, P.; Ritz, T.; Wiltschko, R.; Wiltschko, W. *Planta* **2007**, *225*, 615.

(5) Yoshii, T.; Ahmad, M.; Helfrich-F.rster, C. *PLoS Biol.* **2009**, *7*, e1000086.

(6) Essen, L.-O. *Curr. Opin. Struct. Biol.* **2006**, *16*, 51.

(7) Kottke, T.; Batschauer, A.; Ahmad, M.; Heberle, J. *Biochemistry* **2006**, *45*, 2472.

(8) Brautigam, C. A.; Smith, B. S.; Ma, Z.; Palnitkar, M.; Tomchick, D. R.; Machius, M.; Deisenhofer, J. *Proc. Nat. Acad. Sci. U.S.A.* **1997**, *101*, 9811.

(9) Solov'yov, I. A.; Chandler, D. E.; Schulten, K. *Biophys. J.* **2007**, *92*, 2711.

(10) Timmel, C. R.; Till, U.; Brocklehurst, B.; McLauchlan, K. A.; Hore, P. J. *Mol. Phys.* **1998**, *95*, 71.

(11) Rodgers, C. T.; Norman, S. A.; Henbest, K. B.; Timmel, C. R.; Hore, P. J. *J. Am. Chem. Soc.* **2007**, *129*, 6746.

(12) Till, U.; Timmel, C.; Brocklehurst, B.; Hore, P. *Chem. Phys. Lett.* **1998**, *298*, 7.

(13) Kao, Y.-T.; Tan, C.; Song, S.-H.; Otürk, N.; Li, J.; Wang, L.; Sancar, A.; Zhong, D. *J. Am. Chem. Soc.* **2008**, *130*, 7695.

(14) Efimova, O.; Hore, P. J. *Biophys. J.* **2008**, *94*, 1565.

(15) Zeugner, A.; Byrdin, M.; Bouly, J. P.; Bakrim, N.; Giovani, B.; Brettel, K.; Ahmad, M. *J. Biol. Chem.* **2005**, *280*, 19437.

(16) Bouly, J.-P.; Schleicher, E.; Dionisio-Sese, M.; Vandenbussche, F.; Straeten, D. V. D.; Bakrim, N.; Meier, S.; Batschauer, A.; Galland, P.; Bittl, R.; et al. *J. Biol. Chem.* **2007**, *282*, 9383.

(17) Byrdin, M.; Eker, A. P. M.; Vos, M. H.; Brettel, K. *Proc. Natl. Acad. Sci. U.S.A.* **2003**, *100*, 8676.

(18) In addition, the nuclear quadrupole interaction has been examined recently by Efimova and Hore.[45] It has been shown that this interaction is unimportant for magnetic response of the FAD-Trp radical pairs.

(19) DeVault, D. *Quantum mechanical tunneling in biological systems*; Cambridge University Press: Cambridge, 1984.

(20) Himo, F.; Eriksson, L. A. *J. Phys. Chem. B* **1997**, *101*, 9811.

(21) Lendzian, F.; Sahlin, M.; MacMillan, F.; Bittl, R.; Fiege, R.; Potsch, S.; Sjoberg, B.-M.; Graslund, A.; Lubitz, W.; Lassmann, G. *J. Am. Chem. Soc.* **1996**, *118*, 8111.

(22) Barone, V. In *Recent Advances in Density Functional Methods, Part I*; Chong, D. P., Ed.; World Scientific: Singapore, 1995; p 287.

(23) Munzarová, M. In *Calculation of NMR and EPR Parameters: Theory and Applications*; Kaupp, M., Bühl, M., Malkin, V. G., Eds.; Wiley-VCH: Weinheim, 2004; p 463.

(24) Frisch, M. J.; Trucks, G. W.; Schlegel, H. B.; Scuseria, G. E.; Robb, M. A.; Cheeseman, J. R.; Montgomery, J. A., Jr.; Vreven, T.; Scalmani, G.; Mennucci, B.; Barone, V.; Petersson, G. A.; Caricato, M.; Nakatsuji, H.; Hada, M.; Ehara, M.; Toyota, K.; Fukuda, R.; Hasegawa, J.; Ishida, M.; Nakajima, T.; Honda, Y.; Kitao, O.; Nakai, H.; Li, X.; Hratchian, H. P.; Peralta, J. E.; Izmaylov, A. F.; Kudin, K. N.; Heyd, J. J.; Brothers, E.; Staroverov, V. N.; Zheng, G.; Kobayashi, R.; Normand, J.; Sonnenberg, J. L.; Ogliaro, F.; Bearpark, M.; Parandekar, P. V.; Ferguson, G. A.; Mayhall, N. J.; Iyengar, S. S.; Tomasi, J.; Cossi, M.; Rega, N.; Burant, J. C.; Millam, J. M.; Klene, M.; Knox, J. E.; Cross, J. B.; Bakken, V.; Adamo, C.; Jaramillo, J.; Gomperts, R.; Stratmann, R. E.; Yazyev, O.; Austin, A. J.; Cammi, R.; Pomelli, C.; Ochterski, J. W.; Ayala, P. Y.; Morokuma, K.; Voth, G. A.; Salvador, P.; Dannenberg, J. J.; Zakrzewski, V. G.; Dapprich, S.; Daniels, A. D.; Strain, M. C.; Farkas, O.; Malick, D. K.; Rabuck, A. D.; Raghavachari, K.; Foresman, J. B.; Ortiz, J. V.; Cui, Q.; Baboul, A. G.; Clifford, S.; Cioslowski, J.; Stefanov, B. B.; Liu, G.; Liashenko, A.; Piskorz, P.; Komaromi, I.; Martin, R. L.; Fox, D. J.; Keith, T.; Al-Laham, M. A.; Peng, C. Y.; Nanayakkara, A.; Challacombe, M.; Chen, W.; Wong, M. W.; Pople J. A. *Gaussian Development Version, Revision G.03+*; Gaussian, Inc.: Wallingford, CT, 2008.

(25) Stratmann, R. E.; Scuseria, G. E.; Frisch, M. J. *J. Chem. Phys.* **1998**, *109*, 8218.

(26) Dyall K. G.; Faegri, K., Jr. *Introduction to relativistic quantum chemistry*; Oxford University Press: New York, 2006.

(27) Harriman, J. E. *Theoretical Foundations of Electron Spin Resonance*; Academic Press: New York, 1978.

(28) Gilka, N.; Taylor, P. R.; Marian, C. M. *J. Chem. Phys.* **2008**, *129*, 044102.

(29) Ganyushin, D.; Neese, F. *J. Chem. Phys.* **2006**, *125*, 024103.

(30) Neese, F. *J. Chem. Phys.* **2007**, *127*, 164112.

(31) Foresman, J. B.; Head-Gordon, M.; Pople, J. A.; Frisch, M. J. *J. Phys. Chem.* **1992**, *96*, 135.

(32) Sinnecker, S.; Neese, F. *J. Phys. Chem. A* **2006**, *110*, 12267.

(33) Koseki, S.; Schmidt, M. W.; Gordon, M. S. *J. Phys. Chem.* **1992**, *96*, 10768.

(34) Landau, L. D.; Lifshitz, E. M. *Quantum mechanics: non-relativistic theory*; Pergamon Press: Oxford and New York, 1977.

(35) Neese, F.; Solomon, E. I. *Inorg. Chem.* **1998**, *37*, 6568.
(36) The exponents have been obtained by least-square fitting of $\log(R)-\log(D)$ three point plots.
(37) Connor, H. D.; Sturgeon, B. E.; Mottley, C.; Jr, H. J. S.; Mason, R. P. *J. Am. Chem. Soc.* **2008**, *130*, 6381.
(38) $1\ \mathrm{G} \approx 0.93 \times 10^{-4}\ \mathrm{cm}^{-1}$.
(39) Biskup, T.; Schleicher, E.; Okafuji, A.; Link, G.; Hitomi, K.; Getzoff, E. D.; Weber, S. *Angew. Chem., Int. Ed.* **2009**, *48*, 404.
(40) Bittl, R.; Weber, S. *Biochim. Biophys. Acta Bioenerg.* **2005**, *1707*, 117.
(41) We used $\langle\Phi|S_z|\Phi\rangle = 1/2$ in eqs 27 and 28 because unpaired electrons are well separated and interact with two different sets of nuclei.
(42) Ritz, T.; Wiltschko, R.; Hore, P.; Rodgers, C. T.; Stapput, K.; Thalau, P.; Timmel, C. R.; Wiltschko, W. *Biophys. J.* **2009**, *96*, 3451.
(43) Solov'yov, I. A.; Chandler, D. E.; Schulten, K. *Plant Signaling Behav.* **2008**, *3*, 676.
(44) Solov'yov, I. A.; Schulten, K. *Biophys. J.* **2009**, *96*, 4804.
(45) Efimova, O.; Hore, P. J. *Mol. Phys.* **2009**, *107*, 665.

JP900357F